



## OPEN

## Size-dependent giant-magnetoresistance in millimeter scale GaAs/AlGaAs 2D electron devices

R. G. Mani<sup>1</sup>, A. Kriisa<sup>2</sup> & W. Wegscheider<sup>3</sup><sup>1</sup>Dept. of Physics and Astronomy, Georgia State University, Atlanta, GA 30303 U.S.A., <sup>2</sup>Department of Physics, Emory University, Atlanta, GA 30322 U.S.A., <sup>3</sup>Laboratorium für Festkörperphysik, ETH Zürich, 8093 Zürich, Switzerland.

Received

29 April 2013

Accepted

4 September 2013

Published

25 September 2013

Correspondence and requests for materials should be addressed to R.G.M. (mani.rg@gmail.com)

Large changes in the electrical resistance induced by the application of a small magnetic field are potentially useful for device-applications. Such Giant Magneto-Resistance (GMR) effects also provide new insights into the physical phenomena involved in the associated electronic transport. This study examines a “bell-shape” negative GMR that grows in magnitude with decreasing temperatures in *mm*-wide devices fabricated from the high-mobility GaAs/AlGaAs 2-Dimensional Electron System (2DES). Experiments show that the span of this magnetoresistance on the magnetic-field-axis increases with decreasing device width, *W*, while there is no concurrent Hall resistance,  $R_{xy}$ , correction. A multi-conduction model, including negative diagonal-conductivity, and non-vanishing off-diagonal conductivity, reproduces experimental observations. The results suggest that a size effect in the *mm*-wide 2DES with *mm*-scale electron mean-free-paths is responsible for the observed “non-ohmic” size-dependent negative GMR.

Giant magnetoresistance(GMR) due to spin transport in metallic magnetic multilayers is a well known spintronics effect that finds large volume applications in the read-head of computer hard disks<sup>1,2</sup>. GMR also occurs in semiconductors, and semiconductor GMR is interesting from both the sensing-application<sup>-3</sup> and basic-physics- perspectives<sup>4-21</sup>. Physically, semiconductor - magnetoresistance is interesting because it can provide insight into localization and scattering in disordered 2D electronic systems<sup>4</sup>. Noteworthy topics here include weak localization<sup>4,11</sup>, weak anti-localization<sup>4,11</sup>, electron-electron interaction-induced magnetoresistance<sup>4,6,8-10,12,14,16,18</sup>, metal-insulator transitions induced by a magnetic field<sup>22</sup>, and GMR in the quantum Hall regime<sup>23-25</sup>.

Improvements in the material quality of the GaAs/AlGaAs 2DES, with two-dimensional electron mobilities,  $\mu_0$ , now routinely exceeding the  $10^7$   $cm^2/Vs$  level have helped to study unexpected physical phenomena such as, for example, the microwave radiation-induced zero-resistance states<sup>26</sup>. Here, we examine a “bell-shape” negative GMR effect confined to  $B \leq 0.1$  T that grows in magnitude with decreasing temperatures, *T*, in the same high mobility GaAs/AlGaAs 2DES<sup>8,12,14,17,19-21</sup>. In devices sharing the same material characteristics at a constant temperature, *T*, we show that the span on the magnetic field, *B*, axis of the negative magnetoresistance increases with decreasing device width, *W*, without concurrent Hall resistance corrections, in millimeter-sized devices. A multi-conduction model captures the essential features of experiment. The results suggest that a “non-ohmic” temperature- and size- dependent negative diagonal conductivity term, possibly due to boundary-scattering-induced transport-constriction, might be responsible for the observed negative GMR effect. The results also serve to propose the possibility of novel zero-resistance states arising from such a negative magnetoresistance effect.

## Results

**Size-dependent GMR.** Figure 1 exhibits the measured diagonal magnetoresistance,  $R_{xx}$ , of a triple Hall bar device, with non-invasive probes<sup>27,28</sup>, that is illustrated on the right side of Fig. 1. The length-to-width ratio  $L/W = 1$  for each section. Panels (a), (b), and (c) of Fig. 1 show  $R_{xx}$  vs. the magnetic field, *B*, for  $-0.15 \leq B \leq 0.15$  Tesla, over the temperature range  $1.4 \leq T \leq 6.35$  K, for the  $W = 0.4, 0.2,$  and  $0.1$  *mm*-wide devices, respectively. Fig. 1(a) also exhibits the linear Hall resistance  $R_{xy}$  vs. *B* for the  $W = 0.4$  *mm* section. In all three panels, a positive magnetoresistance is evident at the highest temperature. As *T* is reduced, the  $R_{xx}$  at  $B = 0$  Tesla decreases, and at the same time, negative magnetoresistance contributions become stronger with decreasing temperature. A close examination of the data indicates that two distinct negative magnetoresistance terms are discernable in Fig. 1(b) and (c). A first small negative magnetoresistance term (see also ref. 20), which will be examined in greater detail

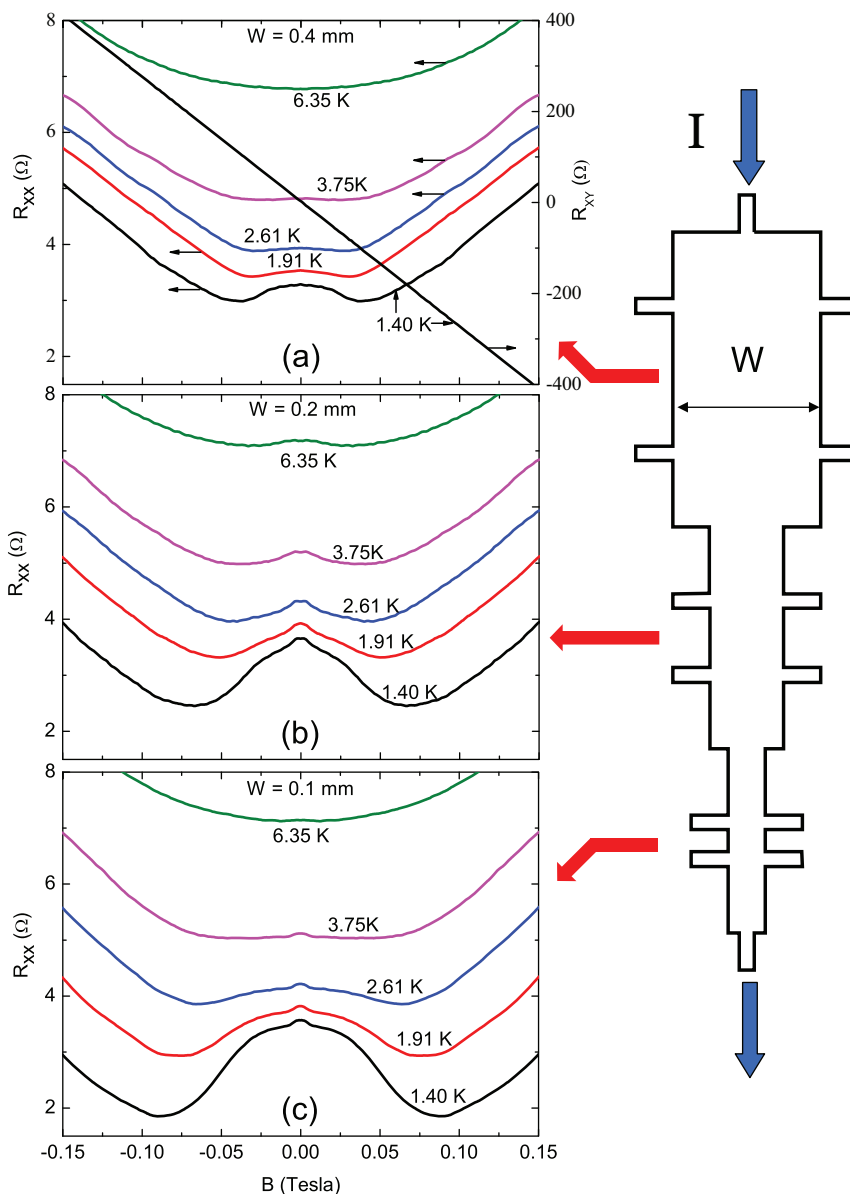


**Figure 1** | Right: A sketch of the GaAs/AlGaAs Hall bar sample including three sections, from top to bottom, with width  $W = 0.4, 0.2,$  and  $0.1$  mm, respectively. (a) This panel shows  $R_{xx}$  [left-ordinate] and  $R_{xy}$  [right-ordinate] vs. the magnetic field,  $B$ , for the  $W = 0.4$  mm section. (b)  $R_{xx}$  vs.  $B$  for the  $W = 0.2$  mm section. (c)  $R_{xx}$  vs.  $B$  for the  $W = 0.1$  mm section. The parameter appearing next to the data traces is the temperature,  $T$ , as indicated. These data suggest that a bell-shape magneto-resistance becomes wider with decreasing  $W$ , at each  $T$ .

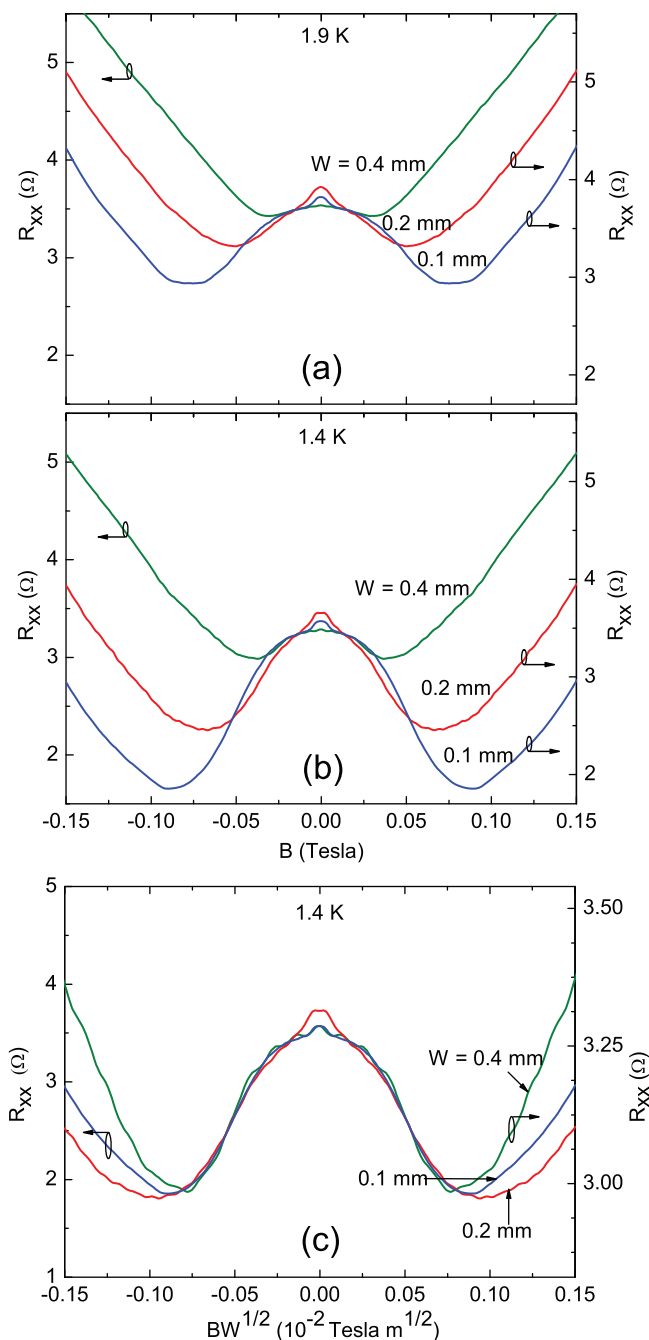
elsewhere, is restricted to  $B \leq 0.01$  Tesla. A larger second term, which is the focus of this study, spans a wider  $B$  field range,  $-0.1 < B < 0.1$  Tesla in Fig. 1(c), and exhibits the greater magnetoresistive contribution at the lowest  $T$ . For  $W = 0.1$  mm, this term produces a nearly 50 per-cent reduction in  $R_{xx}$  over  $B \leq 0.1$  Tesla, clearly a GMR effect. This negative GMR term will be referred to here as the “bell-shape” magnetoresistance. A comparison of panels (a), (b), and (c) also shows that, at a const  $T$ , the typical width of this negative magnetoresistance contribution becomes larger at smaller device widths. Thus, these results empirically establish a size-dependent negative magnetoresistance effect in this high mobility GaAs/AlGaAs system.

Figure 2(a) exhibits a direct comparison of the  $R_{xx}$  for the three Hall bar sections of Fig. 1 at  $T = 1.9$  K. Figure 2(b) exhibits a similar comparison at  $T = 1.4$  K. The striking feature observable in Fig. 2(a) and 2(b) is that the characteristic field scale for the “bell-shape” negative magnetoresistance is strongly dependent upon the device width, as mentioned above. In order to illustrate that the functional

form of the magnetoresistance is the same in the three devices, we re-plot in Fig. 2(c) the data of Fig. 2(b) as  $R_{xx}$  vs  $BW^{1/2}$ , where  $W$  is the device width. In Fig. 2(c), there is observable data collapse onto the same bell shape envelope over  $-0.075 \leq BW^{1/2} \leq 0.075$  ( $\times 10^{-2}$  Tesla  $m^{1/2}$ ). Note that a necessary condition for observing such behavior is that the devices being subjected to the comparison exhibit at least the same macroscopic material characteristics, characteristics that can also depend upon the temperature.

A question that arises at this point is whether there is a Hall effect correction associated with the bell-shape negative magnetoresistance effect. The next section addresses this point.

**Study of the Hall effect correction due to the bell-shape negative magnetoresistance effect.** Figure 3 exhibits the data for a  $W = 0.2$  mm wide Hall bar at dilution refrigerator temperatures,  $T < 0.6$  K. In this sample, see Fig. 3(a), the negative magnetoresistance effect is most pronounced below  $0.6$  K. The concurrently measured  $R_{xy}$ , offset for clarity and exhibited in Fig. 3(b), show linearity as in



**Figure 2** | (a) This panel compares the  $R_{xx}$  vs.  $B$  for  $W = 0.4, 0.2$ , and  $0.1\text{ mm}$  sections at  $1.9\text{ K}$ . The panel suggests a monotonic increase in the full-width at half-maximum of the bell-shape magneto-resistance, with decreasing  $W$ . (b) This panel compares the  $R_{xx}$  vs.  $B$  for  $W = 0.4, 0.2$ , and  $0.1\text{ mm}$  sections at  $1.4\text{ K}$ . (c) At  $1.4\text{ K}$ ,  $R_{xx}$  has been plotted vs.  $BW^{1/2}$  in order to convey data collapse of the bell-shape magneto-resistance observed for  $W = 0.4, 0.2$ , and  $0.1\text{ mm}$ -wide Hall bars. Here, the ordinate scale for the  $W = 0.2\text{ mm}$  device is not shown.

Fig. 1(a), without any noticeable variation over the entire temperature range. Fig. 3(c) shows  $\Delta R_{xy} = R_{xy} - R_{xy}(0.59\text{ K})$ , with the traces offset for clarity. This figure shows that there is no noticeable change in  $R_{xy}$  as the  $R_{xx}$  develops the negative GMR with the reduction in  $T$ . Thus, it appears that  $R_{xy}$  corrections are not induced by the observed bell-shape negative magnetoresistance effect.

**Model and data-fit.** As mentioned, there are two distinct magnetoresistances observable in the data: A first, small, negative magnetoresistance

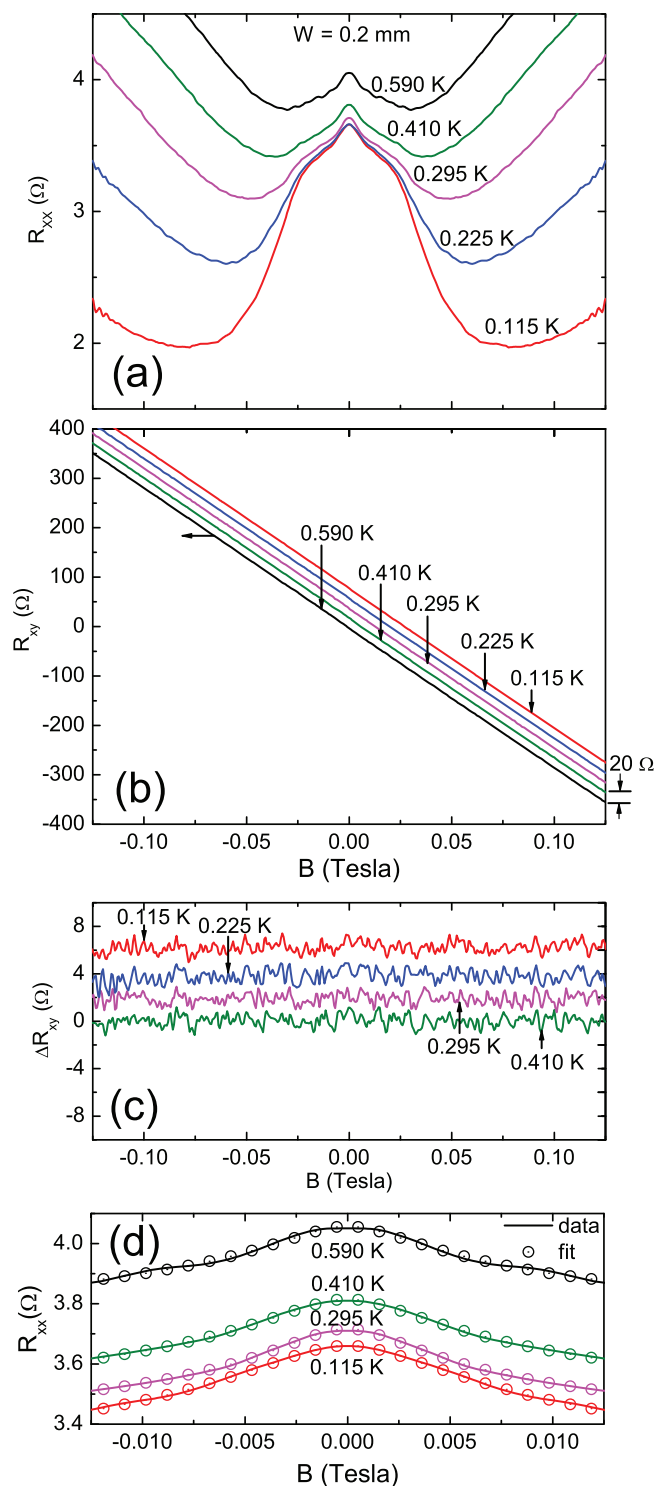


**Figure 3** | (a) This panel shows  $R_{xx}$  vs. the magnetic field,  $B$ , for a  $W = 0.2\text{ mm}$  Hall bar device at  $T < 0.6\text{ K}$ . (b) This plot shows  $R_{xy}$  vs.  $B$  for the same device. Here, the data traces have been offset vertically by  $20\text{ }\Omega$  for the sake of presentation. (c) This plot, which shows  $\Delta R_{xy} = R_{xy} - R_{xy}(0.59\text{ K})$  vs.  $B$ , indicates the absence of  $T$ -dependent  $R_{xy}$  corrections, with respect to the  $T = 0.59\text{ K}$  trace, in this low magnetic field regime. Here, the data traces for  $T = 0.115, 0.225$ , and  $0.295\text{ K}$  have been offset vertically for the sake of presentation. (d) The small resistance ( $R_{xx}$ ) peak observed for  $B \leq 0.01\text{ Tesla}$  in panel (a) is plotted here on an expanded scale. Also shown are fits to the data using 2D weak localization theory. The good agreement between data and fit suggests that the small magnetoresistance peak may be attributed to weak localization.



term, which is restricted to approximately  $B \leq 0.01$  Tesla, and a second larger bell-shape negative magnetoresistance that extends to  $B \approx 0.1$  Tesla. As the latter term is the main topic of this paper, we just briefly examine the former term in Fig. 3(d), which exhibits an expanded plot of the small negative magnetoresistance term from Fig. 3(a). Also shown in Fig. 3(d) are fits to this small magnetoresistance term using 2D weak localization theory neglecting spin-orbit and spin scattering, see eqn. 3.24b in ref. 11. The good agreement between data and the weak localization fit observed here suggest that the small magnetoresistance term may be attributed to weak localization. As a consequence, for the remainder of this discussion, we ignore the small term, and focus solely on the larger bell-shape magnetoresistance.

We have found that a semi-empirical multi-conduction model is able to simulate the observed bell-shape negative magnetoresistance in the magneto-transport. The results are summarized below. In a homogeneous 2D Hall bar specimen, the diagonal resistance  $R_{xx} = \rho_{xx}(L/W)$ , where  $\rho_{xx}$  is the diagonal resistivity, and  $L/W$  is device length-to-width ratio. Since  $L/W = 1$  for the devices in Fig. 1 and 2, we set  $R_{xx} = \rho_{xx}$  and model  $\rho_{xx}$ . The multi-conduction model utilized here invokes three conduction terms, and evaluates  $\rho_{xx}$  and the off-diagonal resistivity,  $\rho_{xy}$  in terms of the diagonal,  $\sigma_{xx}$  and off-diagonal,  $\sigma_{xy}$  conductivities, respectively, via eqns. 1 and 2.

$$\rho_{xx} = \sigma_{xx} / \left[ \sigma_{xx}^2 + \sigma_{xy}^2 \right] \quad (1)$$

$$\rho_{xy} = \sigma_{xy} / \left[ \sigma_{xx}^2 + \sigma_{xy}^2 \right] \quad (2)$$

Since conductivities are additive, the total diagonal conductivity,  $\sigma_{xx}$ , is given by eqn. 3.

$$\sigma_{xx} = \sum_{i=0}^2 \sigma_{xx}^i = \sum_{i=0}^2 \sigma_i / [1 + (\mu_i B)^2] \quad (3)$$

Similarly,  $\sigma_{xy}$  is given by eqn. 4.

$$\sigma_{xy} = \sum_{i=0}^2 \sigma_{xy}^i = \sum_{i=0}^2 \sigma_i \mu_i B / [1 + (\mu_i B)^2] \quad (4)$$

Here, the zeroth terms,  $\sigma_{xx}^0$  and  $\sigma_{xy}^0$ , represent the high mobility electrons in the 2D-electron system and, therefore,  $\sigma_0 = n_0 e \mu_0$  where  $n_0$  and  $\mu_0$  correspond to the 2D electron density and the mobility, respectively. A single conduction model with  $B$ -independent parameters is known to model a constant  $\rho_{xx}$  and a linear-in- $B$  off-diagonal Hall resistivity,  $\rho_{xy}$ . The experimental results at the highest temperature, e.g.,  $T = 6.35$  K in Fig. 1(a), show, however, a parabolic positive magnetoresistance. To account for this effect, we introduced the first term denoted by  $\sigma_{xx}^1$  and  $\sigma_{xy}^1$  in the multi-conduction model.

As mentioned, the data indicate, in addition, a bell-shape negative GMR with the reduction of the temperature. To account for this bell-shape negative magnetoresistance, we introduced a second term given by  $\sigma_{xx}^2$  and  $\sigma_{xy}^2$ . For this second term, a search over the parameter space suggested the possibility of realizing bell-shape negative magnetoresistance with  $\sigma_2 < 0$  only. Since conductivities are additive, a negative  $\sigma_2$  indicates the total conductivity is reduced by such a term. Note that, unlike the zeroth term, both the first and second terms are described by conductivities  $\sigma_1$ ,  $\sigma_2$  and mobilities  $\mu_1$ ,  $\mu_2$ , respectively. These finite mobilities indicate that there is a non-vanishing off-diagonal conductivity associated with each term as  $\sigma_{xy}^i = \sigma_{xx}^i \times \mu_i B$ .

Figure 4(a) shows least squares fits of the  $R_{xx}$  vs.  $B$  data traces for the  $W = 0.2$  mm Hall bar section of Fig. 1, using eqns. 1–4. In Fig. 4(a), the data are indicated by the solid lines and the fits are indicated by symbols. Note that this model does not capture the small negative magnetoresistance term mentioned earlier that is confined to  $B \leq 0.01$  Tesla, since we ignored this weak localization term in the fitting here. The figure suggests that, otherwise, this model provides a good description of the data. Similar fits were also carried out for the

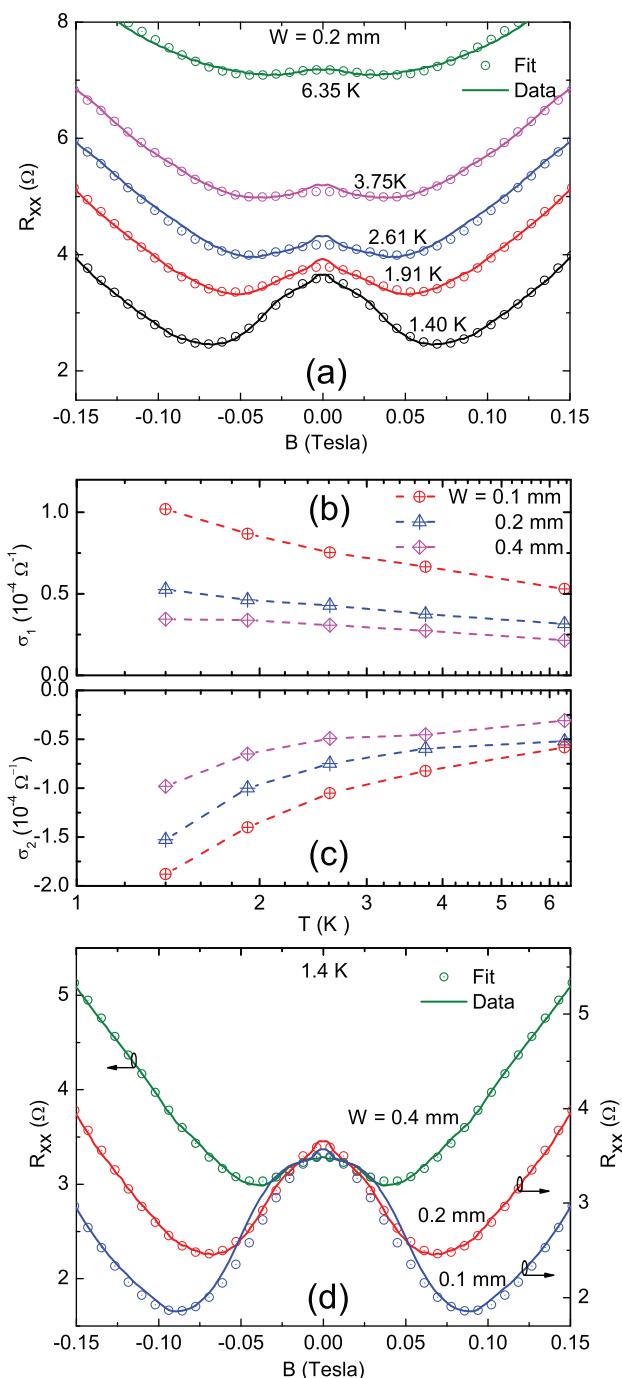


**Figure 4** | (a) This panel shows  $R_{xx}$  vs.  $B$  for the  $W = 0.2$  mm Hall bar section of Fig. 1. Also shown are fits to the data using a multi-conduction model, see text. Associated fit parameters are presented in Table 1. (b) This panel presents the fit parameter  $\sigma_1$  extracted from data fits for the three device sections of Fig. 1. (c) This panel presents the fit parameter  $\sigma_2$  extracted from data fits for the three device sections of Fig. 1. In (b) and (c), note the size and temperature dependence in  $\sigma_1$  and  $\sigma_2$ . Note also that temperature is indicated here on a logarithmic scale. (d) This panel presents the  $R_{xx}$  vs.  $B$  for  $W = 0.4$ ,  $0.2$ , and  $0.1$  mm device sections of Fig. 1 at  $1.4$  K. Also shown are fits to the data using the multi-conduction model, see text. Associated fit parameters are presented in Table 2.

$W = 0.1$  mm and  $W = 0.4$  mm data of Fig. 1. The results indicated similar good agreement between data and fit.

At the outset, there are six parameters,  $n_0$ ,  $\mu_0$ ,  $\sigma_1$ ,  $\mu_1$ ,  $\sigma_2$ , and  $\mu_2$ , in these fits. The number of free parameters has been reduced, however,





**Table 1** | Fit parameters for the data-fits shown in Figure 4(a), for the  $R_{xx}$  vs.  $B$  data traces of the  $W = 0.2$  mm wide Hall bar at various temperatures. Here, the parameters  $n_0$ ,  $\mu_1$ , and  $\mu_2$  were held constant at the indicated values.  $n_0$  is given in units of  $10^{11} \text{ cm}^{-2}$  and  $\mu_0$ ,  $\mu_1$  and  $\mu_2$  are given in units of  $10^6 \text{ cm}^2/\text{Vs}$

T(K)	$n_0$	$\mu_0$	$\sigma_1(\Omega^{-1})$	$\mu_1$	$\sigma_2(\Omega^{-1})$	$\mu_2$
1.40	2.29	7.59	$5.26 \times 10^{-5}$	0.059	$-15.3 \times 10^{-5}$	0.14
1.91	2.29	7.21	$4.63 \times 10^{-5}$	0.059	$-10.0 \times 10^{-5}$	0.14
2.61	2.29	6.55	$4.29 \times 10^{-5}$	0.059	$-7.48 \times 10^{-5}$	0.14
3.75	2.29	5.37	$3.75 \times 10^{-5}$	0.059	$-5.95 \times 10^{-5}$	0.14
6.35	2.29	3.80	$3.15 \times 10^{-5}$	0.059	$-5.19 \times 10^{-5}$	0.14

by applying constraints. For example,  $n_0$  is extracted from the Hall effect measurement and held to the associated value throughout the fits. Similarly,  $\mu_0$ , the Hall mobility is constrained by the dc-resistivity measurement and the variation of  $\mu_0$  with  $T$  is determined by the  $T$  variation of the dc-resistivity. Further, for the sake of simplicity,  $\mu_1$  and  $\mu_2$  were held constant vs.  $T$ . Thus, for the fits to the  $T$ -dependent data, only two parameters were allowed to vary with  $T$  without constraint:  $\sigma_1$  and  $\sigma_2$ .

The parameters for the fits shown in Fig. 4(a) are tabulated in Table 1. The simulations indicated that the inclusion of the first term, i.e.,  $\sigma_{xx}^1$  and  $\sigma_{xy}^1$ , with a  $\sigma_1 > 0$  and  $\mu_1 = \text{constant} = 0.059 \times 10^6 \text{ cm}^2/\text{Vs}$ , see Table 1, makes possible a description of the observed positive magnetoresistance at all exhibited  $T$ . A plot of  $\sigma_1$  vs.  $T$  for the  $W = 0.1, 0.2$ , and  $0.4$  mm Hall bar sections of Fig. 1 is provided in Fig. 4(b).

The fit extracted values for  $\sigma_2$  and  $\mu_2$ , given in Table 1, show that the observed bell shape negative magnetoresistance can be fit with  $\mu_2 = \text{constant} = 0.14 \times 10^6 \text{ cm}^2/\text{Vs}$  over the entire  $T$ -range. The increasing magnitude of the bell-shape GMR with decreasing  $T$  is therefore attributed to the increasing magnitude of  $\sigma_2$ , which is negative, with decreasing  $T$ . A plot of  $\sigma_2$  vs.  $T$  for the  $W = 0.1, 0.2$  and  $0.4$  mm Hall bar sections of Fig. 1 is provided in Fig. 4(c). Note the size- and  $T$ -dependence of  $\sigma_2$  in Fig. 4(c).

Fig. 4(d) provides a comparative plot of the data and fit results for the  $W = 0.1, 0.2$  and  $W = 0.4$  mm Hall bars sections of Fig. 1 at  $T = 1.4$  K; this plot exhibits good agreement between data and the fit in all three cases. The associated fit parameters are given in Table 2. Here, the  $\mu_1$ , which represents the positive magnetoresistance term, takes on the same value for the three Hall bar sections, while  $\sigma_1$  increases with decreasing  $W$ . Next,  $\sigma_2$  is negative and increases in magnitude with decreasing  $W$ , while  $\mu_2 \propto W^{1/2}$ . The latter feature is consistent with the data collapse exhibited in Fig. 2(c), while the former is consistent with broader and deeper bell-shape negative GMR at smaller Hall bar widths, see also Fig. 1. Finally, the size dependence of  $\mu_2$  and the smaller  $\mu_2$  in the smaller devices suggests increased transport constriction due to boundary scattering in smaller devices.

Results of a similar analysis are shown in Fig. 5 for the transport data obtained below 1 K for a single Hall bar specimen ( $L/W = 1$ ) with  $W = 0.4$  mm fabricated from GaAs/AlGaAs material exhibiting  $\mu_0 = 1 \times 10^7 \text{ cm}^2/\text{Vs}$  and  $n_0 = 1.9 \times 10^{11} \text{ cm}^{-2}$ . From Fig. 5(a), it is evident that, at  $T = 0.15$  K,  $R_{xx}(B = 0.065 \text{ T})$  is merely  $\approx 50\%$  of  $R_{xx}(B = 0)$  - a signature of a GMR effect. Further, here, the  $R_{xx}(B = 0)$  is approximately insensitive to  $T$  because  $\mu_0 \approx \text{constant}$ , unlike in the data of Fig. 1 and Fig. 3. The fit-results, also plotted in Fig. 5(a), show good agreement between data and model. The fit parameters  $\sigma_1$  and

$\sigma_2$  obtained from the fits are exhibited as a function of  $T$ , on a logarithmic scale, in Fig. 5(b). This plot shows that  $\sigma_1$ , which characterizes the positive magnetoresistance, is constant, while  $\sigma_2 \leq 0$ , and increases in magnitude with decreasing temperatures below 1 K, followed by saturation at the lowest  $T$ . Note that, in this specimen, the bell-shape negative magnetoresistance showed saturation and did not grow larger with decreasing temperatures below  $T \approx 0.2$  K. Fig. 5(c) exhibits the Hall resistance  $R_{xy}$  vs.  $B$  at five temperatures. Again, the  $R_{xy}$  measurements indicated a linear Hall effect down to the 0.5 per-cent level, and a temperature dependent  $R_{xy}$  correction was not observed. The multi-conduction model, eqns. 1–4, succeeded in describing the observed  $R_{xy}$ , with the same parameters as for the  $R_{xx}$  fits of Fig. 5(a). A  $R_{xy}$  fit at  $T = 0.15$  K is also exhibited in Fig. 5(c).

**Zero-resistance state (ZRS).** Next, we address the question whether, due to the observed negative GMR, a specimen that exhibits non-zero  $R_{xx}$  at  $B = 0$  can exhibit vanishing diagonal resistance in a perpendicular magnetic field<sup>26</sup>. To answer this question, we present some results obtained using the multiconduction model presented above. Consider first the case where the positive magnetoresistance term can be neglected, i.e.,  $\sigma_1 = 0$ . Then, vanishing  $\rho_{xx}$  can be obtained in a large  $B$  limit within the model when  $\sigma_2/\mu_2^2 = \sigma_0/\mu_0^2$ . A model simulation of  $R_{xx}$  with  $\sigma_1 = 0$  is shown for parameters satisfying the above-mentioned condition as the red curves in Fig. 6. Note that, in the high- $B$  limit, as defined by the context of such experiments, a vanishing  $R_{xx}$ , indicated as “ZRS” in Fig. 6, can be obtained from the model.

In the second case where  $\sigma_1 \geq 0$ , a positive magnetoresistance is expected to predominate in the high- $B$  limit, based on the experimental observations, see Fig. 1 and Fig. 5(a). Then, vanishing  $R_{xx}$  appears possible, in principle, for a brief  $B$  interval. The blue traces illustrate a model simulation of this scenario in Fig. 6. Note the zero-resistance state in the model simulation in the vicinity of  $B = 0.06$  Tesla without concurrent Hall resistance,  $R_{xy}$ , quantization. Perhaps, in the near future, experiment will allow for the observability of such an equilibrium zero-resistance state in the narrow high mobility 2DES.

## Discussion

Magnetoresistance in the 2DES, over the magnetic field regime examined here, can arise from a number of mechanisms. For example, weak localization or the quantum mechanical coherent backscattering of electrons in a disordered media is a widely observable negative

**Table 2** | Fit parameters for the  $R_{xx}$  data-fits shown in Figure 4(d), for the  $W = 0.4, 0.2$ , and  $0.1$  mm wide Hall bars at  $T = 1.4$  K. For these fits,  $n_0$  and  $\mu_1$  were constants. Note that  $\mu_2 \propto W^{1/2}$ . In the table,  $n_0$  is given in units of  $10^{11} \text{ cm}^{-2}$ , as  $\mu_0$ ,  $\mu_1$  and  $\mu_2$  are given in units of  $10^6 \text{ cm}^2/\text{Vs}$

W( $\mu\text{m}$ )	$n_0$	$\mu_0$	$\sigma_1(\Omega^{-1})$	$\mu_1$	$\sigma_2(\Omega^{-1})$	$\mu_2$
0.4 mm	2.29	8.31	$3.44 \times 10^{-5}$	0.059	$-9.81 \times 10^{-5}$	0.21
0.2 mm	2.29	7.59	$5.26 \times 10^{-5}$	0.059	$-15.3 \times 10^{-5}$	0.14
0.1 mm	2.29	7.80	$10.2 \times 10^{-5}$	0.059	$-18.8 \times 10^{-5}$	0.10

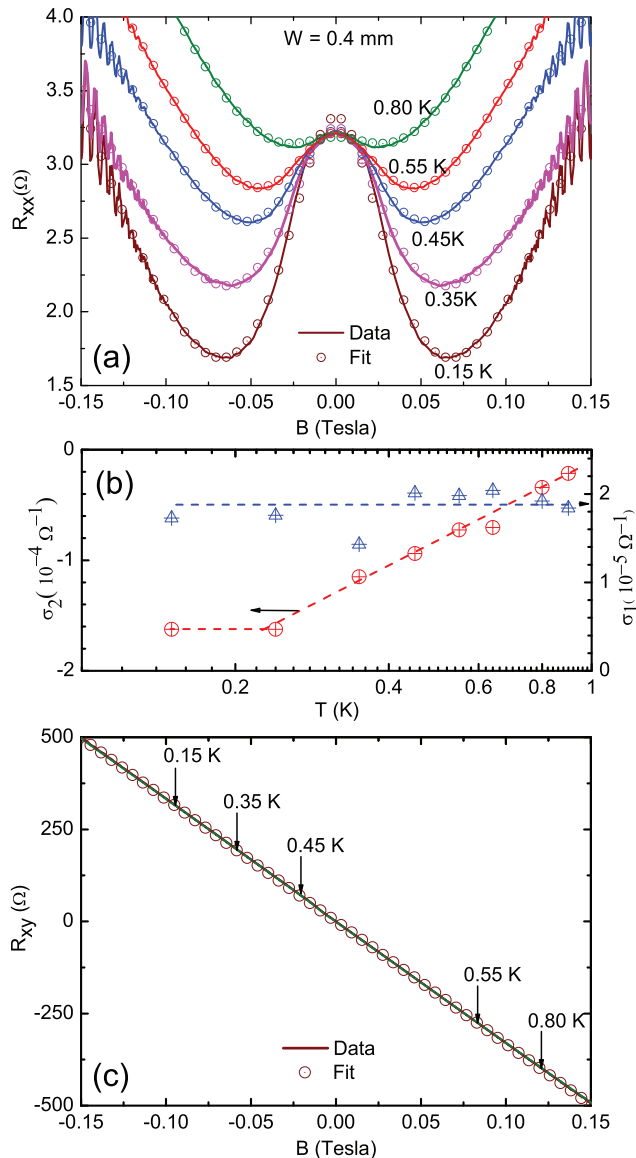


**Figure 5** | (a) This panel shows  $R_{xx}$  vs.  $B$  for a  $W = 0.4$  mm Hall bar for temperatures,  $T \leq 0.8$  K, as indicated. Also shown are fits to the data using a multi-conduction model, see text. (b) The fit extracted conductivities  $\sigma_1$  and  $\sigma_2$ , see text, are shown as a function of the temperature on a logarithmic scale. Here,  $\sigma_1$  represents the positive magnetoresistance term, while  $\sigma_2$  represents the negative magnetoresistance term. (c) This panel shows the  $R_{xy}$  vs.  $B$  measured at various temperatures [solid lines], along with a fit [symbols] for the  $T = 0.15$  K data.  $R_{xy}$  appears insensitive to the temperature.

magnetoresistance correction<sup>4,11</sup>. In systems with strong spin-orbit interaction, coherent backscattering is suppressed rather than enhanced and this leads to a positive magnetoresistance correction known as weak anti-localization<sup>4,11</sup>. Since localization can occur due to both disorder and interaction, interaction counterparts of weak localization, known as the electron-electron interaction corrections were predicted theoretically<sup>4,6,8–10,12,14,18</sup>. Both the interaction and the localization components grow logarithmically with decreasing temperature in two dimensions<sup>4</sup>. Generally, a Hall resistance correction  $\Delta R_{xy}$  is not expected for localization<sup>7</sup>, while a  $\Delta R_{xy}$  correction is expected for the electron-electron interaction effect<sup>10</sup>.

Here, we have examined a bell-shape negative magnetoresistance effect confined to  $B \leq 0.1$  T that grows in magnitude with decreasing temperatures,  $T$ , in the high mobility GaAs/AlGaAs 2DES. The

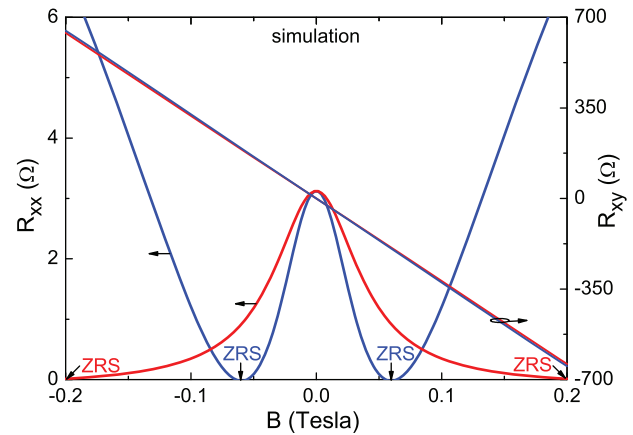


**Figure 6** | Simulations of  $R_{xx}$  vs.  $B$  identify the possibility of a zero-resistance state at a finite  $B$  in a system that exhibits a non-vanishing resistance at  $B = 0$ . Here, the traces in red present a simulation in an effective two-conduction model where the positive magnetoresistance term has been switched off, i.e.,  $\sigma_1 = 0$  and  $\mu_1 = 0$ . The red trace shows  $R_{xx} \rightarrow 0$  in the high- $B$  limit. The traces in blue examine a three-conduction model which includes positive magnetoresistance,  $\sigma_1 > 0$  and  $\mu_1 > 0$ , in the high  $B$ -limit. Here, a zero-resistance state appears possible over a short  $B$  interval, in the vicinity of  $B = 0.06$  Tesla. The red and blue traces share common values for  $n_0$  and  $\mu_0$ :  $n_0 = 2 \times 10^{11} \text{ cm}^{-2}$ ,  $\mu_0 = 10^7 \text{ cm}^2/\text{Vs}$ . For the red traces:  $\sigma_1 = 0$ ,  $\mu_1 = 0$ ,  $\sigma_2 = -2.075 \times 10^{-4} \Omega^{-1}$ , and  $\mu_2 = 2.5 \times 10^5 \text{ cm}^2/\text{Vs}$ . For the blue traces:  $\sigma_1 = 5 \times 10^{-5} \Omega^{-1}$ ,  $\mu_1 = 5 \times 10^4 \text{ cm}^2/\text{Vs}$ ,  $\sigma_2 = -4.4 \times 10^{-4} \Omega^{-1}$ , and  $\mu_2 = 2.5 \times 10^5 \text{ cm}^2/\text{Vs}$ .

precursor of this effect was perhaps first reported by Paalanen et al. in ref. 8 using GaAs/AlGaAs samples with  $1.17 \times 10^{11} \leq n \leq 1.64 \times 10^{11} \text{ cm}^{-2}$  and  $0.65 \times 10^6 \leq \mu \leq 1.64 \times 10^6 \text{ cm}^2/\text{Vs}$ . Subsequently, Choi et al.<sup>12</sup> examined in great detail the electron-electron interactions in the parabolic magnetoresistance in specimens with a higher density and lower mobility than in ref. 8. Mani et al.<sup>14</sup> examined and fit a negative giant magnetoresistance, which is very similar in appearance to the bell-shape negative magnetoresistance reported here, in  $W = 0.2 \mu\text{m}$  wide wires fabricated from  $n = 3 \times 10^{11} \text{ cm}^{-2}$  and  $\mu = 0.5 \times 10^6 \text{ cm}^2/\text{Vs}$  GaAs/AlGaAs material. In modern MBE GaAs/AlGaAs material, i.e., material with mobilities in the  $10^7 \text{ cm}^2/\text{Vs}$  range, Mani et al.<sup>17</sup>, exhibited bell-shape negative magnetoresistance in mm-sized Hall bars amongst results examining the radiation-induced magnetoresistance oscillations, see fig. 2 in ref. 17. Recently, Bockhorn et al.<sup>20</sup> generated new interest in this area by focusing upon the strong temperature- and density-dependent negative magnetoresistance in material characterized by  $n \approx 3.1 \times 10^{11} \text{ cm}^{-2}$  and  $\mu \approx 11.9 \times 10^6 \text{ cm}^2/\text{Vs}$ . They ruled out weak localization as the cause for the small resistance peak and attributed it instead to a ballistic transport effect akin to the quenching of the Hall effect. Further, they fit the parabolic contribution of the huge magnetoresistance with an interaction theory and concluded that the “huge parabolic magnetoresistance is fitted by the interaction correction to the conductivity in the situation of a long-range fluctuation potential and in the regime of ballistic transport and a discrepancy to theory is observed”<sup>20</sup>. Hatke and co-workers<sup>21</sup> examined giant negative magnetoresistance in GaAs/AlGaAs heterostructures ( $n \approx 1.6 \times 10^{11} \text{ cm}^{-2}$  and  $\mu \approx 5.4 \times 10^6 \text{ cm}^2/\text{Vs}$ ) and quantum wells ( $3.4 \times 10^{11} \leq n \leq 4.3 \times 10^{11} \text{ cm}^{-2}$  and  $10 \times 10^6 \leq \mu \leq 12 \times 10^6 \text{ cm}^2/\text{Vs}$ ). They found that the effect is destroyed by increasing temperatures and modest in-plane magnetic fields. They fit the low- $B$  (bell-shape) magnetoresistance with the model  $\rho(B)/\rho_0 = 1 - \beta B^2$ , examined dependence of  $\beta$  on temperature, and compared with predictions for  $\beta$  by the quasiclassical disorder model<sup>15</sup>, and the interaction model<sup>19</sup>. They concluded that the “giant negative magnetoresistance cannot be explained by existing theories considering interaction-induced or



disorder-induced corrections<sup>21</sup>. At this point, it appears worth pointing out that, from the experimental perspective, there is more to the observed bell-shape magnetoresistance than the initial parabolic term. It seems also necessary to account for the saturation of the negative parabolic term, the subsequent positive magnetoresistance, if any, and finally, the observed Hall effect.

So far as the results presented here are concerned, as mentioned in connection with the description of Figure 3, the small negative magnetoresistance term observed for  $B \leq 0.01$  Tesla fits the expectations of weak localization theory, see Fig. 3(d). As a consequence, it appears that weak localization is quenched here above 0.01 Tesla, and therefore, the observed bell-shape negative GMR up to  $B = 0.1$  Tesla cannot be weak localization.

The bell-shape magnetoresistance could have an interaction origin, as often suggested, because the electron-electron interaction correction in the diffusion channel can persist into the strong magnetic field limit, and this point has been used in the past to distinguish the weak localization and electron-electron contributions to the magnetoresistance<sup>4,8,10,12</sup>. However, for electron-electron interactions, theory predicts  $\Delta\sigma_{xy} = 0$ , which implies a temperature dependent correction in  $R_{xy}$  with  $(\delta R_H/R_H^0)/(\delta R/R_0) = 2/(1 - (\omega_c\tau)^2)$ , see eqn. 75–77 in ref. 10. Later developments indicated that the interaction correction to the conductivity  $\delta\sigma$  differed between the diffusive and ballistic regimes, which are distinguished by whether  $k_B T\tau \ll \hbar$  or  $k_B T\tau \geq \hbar$ , respectively<sup>18</sup>. Zala et al. (ref. 16) have examined a parameter,  $\gamma = -\partial_T[\ln\rho_{xy}(T)]/\partial[\ln\sigma_{xx}(T)]$ , and suggested that  $\gamma \rightarrow 0$  for  $k_B T\tau \approx \hbar$ , see Fig. 3, ref. 16.

The results exhibited here indicate that: (i) A  $T$ -dependent  $\Delta R_{xy}$  does not occur in these data, see Fig. 3(c). (ii) Further, the good agreement between data and model-fits suggest there occur corrections in the off-diagonal conductivity,  $\sigma_{xy}$ , in the form of  $\sigma_{xy}^1$  and  $\sigma_{xy}^2$ , in addition to corrections  $\sigma_{xx}^1$  and  $\sigma_{xx}^2$ . This feature, a non-vanishing  $\sigma_{xy}$  correction seems, in our opinion, especially problematic for the canonical electron interaction explanation.

From the analysis presented here, it appears that our multi-conduction model provides a better fit for the experimental data than previous attempts. To our understanding, the improved description of the data is a direct consequence of allowing a non-vanishing off-diagonal conductivity contribution in this context.

At this point one might ask: why does the observed negative magnetoresistance depend upon the device size in Fig. 1? At the outset, one expects to see a size-independent negative magnetoresistance for a size-independent (“ohmic”) conductivity since each device exhibits the same length to width ratio,  $L/W = 1$ . The observed size dependence in  $R_{xx}$ , see Fig. 1, therefore suggests a “non-ohmic” size-dependent correction - one that is sensitive to the ratio between the effective sample size<sup>4</sup>, which is set by a microscopic length scale<sup>4</sup>, and the physical sample size. If the resistance correction depends on the ratio of these two length scales, as envisioned in scaling theories of localization<sup>4,5</sup>, then the observed size dependence, see Fig. 1, 2(a), and 2(b), becomes plausible. That is, in the experimental situation at a constant  $T$ , a temperature dependent microscopic length scale that sets the effective sample size remains invariant across the three device sections, while the physical width varies as indicated, becoming larger in the wider Hall bar sections, and the ratio of these two length scales differs for the three sections of the Hall bar device. Further studies are underway examining the detailed temperature dependence of the  $\sigma_1$  and  $\sigma_2$  to provide more clarity on this matter.

Next, one might ask: What is the physical origin of  $\sigma_2$ , the negative conductivity term? Here, note once again the clear dependence of the bell-shape negative magnetoresistance in Fig. 1 on the size of the Hall bar device, and the larger magnitude conductivity reduction, parameterized by  $\sigma_2$ , in the narrower specimen, see Fig. 4(c). Such results seem to suggest that charge diffusion hindered by boundary scattering might be responsible for the negative  $\sigma_2$  and the associated bell-shape negative GMR.

In summary, millimeter-wide Hall bars fabricated from high mobility GaAs/AlGaAs heterostructures with  $mm$ -scale electron mean free paths exhibit a giant bell-shape negative magnetoresistance at liquid helium temperatures. In devices sharing the same material characteristics at a constant temperature,  $T$ , the characteristic width of the magnetoresistance on the  $B$ -axis increases with decreasing device width,  $W$ . A multi-conduction conduction model, with a negative conductivity,  $\sigma_2$ , negative diagonal conductivity,  $\sigma_{xx}^2$ , and associated non-vanishing off-diagonal conductivity,  $\sigma_{xy}^2$ , captures the essential features of experiment. The results suggest that a small temperature- and size- dependent scattering term might be responsible for the observed negative GMR effect. The multi-conduction model developed here also indicates, see Fig. 6, the possibility of an equilibrium zero-resistance state without Hall resistance quantization at finite  $B$  in the 2DES.

## Methods

**MBE material.** The GaAs/AlGaAs material used in these studies were characterized by a sheet electron density  $1.9 \times 10^{11} \leq n_0(1.5\text{ K}) \leq 2.3 \times 10^{11}\text{ cm}^{-2}$  and an electron mobility  $7.5 \times 10^6\text{ cm}^2/\text{Vs} \leq \mu_0(1.5\text{ K}) \leq 1.1 \times 10^7\text{ cm}^2/\text{Vs}$  after illumination by a red LED to realize the high mobility condition.

**Device fabrication.** Hall bars were fabricated from this material using standard photolithography. The device patterns utilized here included (a) Hall bars of three different widths,  $W = 0.1, 0.2,$  and  $0.4\text{ mm}$ , in series on a single device, see Fig. 1, and (b) Hall bars of a single width,  $W = 0.2\text{ mm}$ , see Fig. 3, and  $W = 0.4\text{ mm}$ , see Fig. 5.

**Length scales.** Note that, at  $n = 2 \times 10^{11}\text{ cm}^{-2}$  and  $\mu = 10^7\text{ cm}^2/\text{Vs}$ , the elastic mean free path  $l_e$  is nearly one-tenth of a millimeter, i.e.,  $l_e = v_f\tau = 0.073\text{ mm}$ , where  $v_f$  is the Fermi velocity, and  $\tau$  is the momentum relaxation time. Thus, in the smallest devices,  $W$  is comparable to  $l_e$ , suggesting quasi-ballistic transport. Further, at low temperatures, the inelastic mean free path,  $l_{in} = v_f\tau_\phi$ , where  $\tau_\phi$  is the inelastic or phase coherence time, can be larger than the  $l_e$  and exceed the device width in the smallest devices.

**Measurement.** For the device pattern exhibited in Fig. 1, all three sections were measured simultaneously at each temperature. The electrical response was measured using low frequency lock-in based techniques. The samples were vapor cooled for  $T > 4.2\text{ K}$ , and immersed in pumped liquid Helium over the range  $1.4 \leq T \leq 4.2\text{ K}$ . For  $T < 1\text{ K}$ , see Fig. 3 and Fig. 5, measurements were carried out with the sample-in-liquid, within the mixing chamber of a dilution refrigerator.

- Baibich, M. N. *et al.* Giant magnetoresistance of (001) Fe/(001) CR magnetic superlattices. *Phys. Rev. Lett.* **61**, 2472–2475 (1988).
- Tsang, C. H. *et al.* Design, fabrication, and performance of spin-valve read heads for magnetic recording applications. *IBM J. Res. Develop.* **42**, 103–116 (1998).
- Heremans, J. Solid state magnetic field sensors and applications. *J. Phys. D: Appl. Phys.* **26**, 1149–1168 (1993).
- Lee, P. A. & Ramakrishnan, T. V. Disordered electronic systems. *Rev. Mod. Phys.* **57**, 287–337 (1985).
- Abrahams, E., Anderson, P. W., Licciardello, D. C. & Ramakrishnan, T. V. Scaling theory of localization: Absence of quantum diffusion in two dimensions. *Phys. Rev. Lett.* **42**, 673–676 (1979).
- Altshuler, B. L., Khmel'nitzkii, D., Larkin, A. I. & Lee, P. A. Magnetoresistance and Hall effect in disordered two-dimensional electron gas. *Phys. Rev. B* **22**, 5142–5153 (1980).
- Fukuyama, H. Hall effect in two-dimensional disordered systems. *J. Phys. Soc. Jpn.* **49**, 644–648 (1980).
- Paalanen, M. A., Tsui, D. C. & Hwang, J. C. M. Parabolic magnetoresistance from the interaction effect in a two-dimensional electron gas. *Phys. Rev. Lett.* **51**, 2226–2229 (1982).
- Girvin, S. M., Jonson, M. & Lee, P. A. Interaction effects in disordered Landau-level systems in two dimensions. *Phys. Rev. B* **26**, 1651–1659 (1982).
- Houghton, A., Senna, J. R. & Ying, S. C. Magnetoresistance and Hall effect of a disordered interacting two-dimensional electron system. *Phys. Rev. B* **25**, 2196–2210 (1982).
- Bergmann, G. Weak localization in thin films - a time-of-flight experiment with conduction electrons. *Phys. Repts.* **107**, 1–58 (1984).
- Choi, K. K., Tsui, D. C. & Palmateer, S. C. Electron-electron interaction in GaAs-AlGaAs heterostructures. *Phys. Rev. B* **33**, 8216–8227 (1986).
- Thornton, T. J., Roukes, M. L., Scherer, A. & van de Gaag, B. P. Boundary scattering in quantum wires. *Phys. Rev. Lett.* **63**, 2128–2131 (1989).
- Mani, R. G., von Klitzing, K. & Ploog, K. Magnetoresistance over the intermediate localization regime in GaAs/AlGaAs quantum wires. *Phys. Rev. B* **48**, 4571–4574 (1993).



15. Mirlin, A. D., Polyakov, D. G., Evers, F. & Wolfe, P. Quasiclassical negative magnetoresistance of a 2D electron gas: Interplay of strong scatterers and smooth disorder. *Phys. Rev. Lett.* **87**, 126805-1-4 (2001).
16. Zala, G., Narozhny, B. N. & Aleiner, I. Interaction corrections to the Hall coefficient at intermediate temperatures. *Phys. Rev. B* **64**, 201201-1-4 (2001).
17. Mani, R. G. *et al.* Magnetoresistive response of a high mobility 2DES under electromagnetic wave excitation. *Physics of Semiconductors 2002 - Proceedings of the 26th International Conference Edinburgh, 29 July - 2 August 2002*, IOP Conf. Series **171**, eds. Long, A. R. and Davies, J. H. (IOP, Bristol, 2003) H112 (arXiv:cond-mat/0305507).
18. Gornyi, I. V. & Mirlin, A. D. Interaction-induced magnetoresistance: From the diffusive to the ballistic regime. *Phys. Rev. Lett.* **90**, 076801-1-4 (2003).
19. Li, L., Proskuryakov, Y. Y., Savchenko, A. K., Linfield, E. H. & Ritchie, D. A. Magnetoresistance of a 2D electron gas caused by electron interactions in the transition from the diffusive to the ballistic regime. *Phys. Rev. Lett.* **90**, 076802-1-4 (2003).
20. Bockhorn, L., Barthold, P., Schuh, D., Wegscheider, W. & Haug, R. J. Magnetoresistance in a high mobility two-dimensional electron gas. *Phys. Rev. B* **83**, 113301-1-4 (2011).
21. Hatke, A. T., Zudov, M. A., Reno, J. L., Pfeiffer, L. N. & West, K. W. Giant negative magnetoresistance in high mobility 2D electron systems. *Phys. Rev. B* **85**, 081304-1-4 (2012).
22. Wang, T., Clark, K. P., Spencer, G. F., Mack, A. M. & Kirk, W. P. Magnetic field induced metal-insulator transition in two dimensions. *Phys. Rev. Lett.* **72**, 709-712 (1994).
23. Das Sarma, S. & Pinczuk, A. *Perspectives in Quantum Hall Effects* (Wiley, New York, 1996).
24. Goldman, V. J., Santos, M., Shayegan, M. & Cunningham, J. E. Evidence for a two-dimensional quantum wigner crystal. *Phys. Rev. Lett.* **64**, 2189-2192 (1990).
25. Santos, M. B. *et al.* Observation of a reentrant insulating phase near the 1/3 fractional quantum Hall liquid in a two-dimensional hole system. *Phys. Rev. Lett.* **68**, 1188-1191 (1992).
26. Mani, R. G. *et al.* Zero-resistance states induced by electromagnetic wave excitation in GaAs/AlGaAs heterostructures. *Nature* **420**, 646-650 (2002).
27. Huard, B., Stander, N., Sulpizio, J. A. & Goldhaber-Gordon, D. Evidence of the role of contacts on the observed electron-hole asymmetry in graphene. *Phys. Rev. B* **78**, 121402 (2008).
28. Mani, R. G., Ghenim, L. & Theis, T. Scaling magnetoresistance induced by superconducting contacts in n-type GaAs. *Phys. Rev. B* **45**, 12098-12101 (1992).

## Acknowledgements

The basic research and helium liquefaction at Georgia State University is supported by the U. S. Department of Energy, Office of Basic Energy Sciences, Material Sciences and Engineering Division, under DE-SC0001762. Work is also supported by the ARO under W911NF-07-01-015.

## Author contributions

The measurements, modeling, and manuscript are due to RGM. AK helped with data fits. The high quality MBE material is due to WW.

## Additional information

**Competing financial interests:** The authors declare no competing financial interests.

**How to cite this article:** Mani, R.G., Kriisa, A. & Wegscheider, W. Size-dependent giant-magnetoresistance in millimeter scale GaAs/AlGaAs 2D electron devices. *Sci. Rep.* **3**, 2747; DOI:10.1038/srep02747 (2013).



This work is licensed under a Creative Commons Attribution-NonCommercial-NoDerivs 3.0 Unported license. To view a copy of this license, visit <http://creativecommons.org/licenses/by-nc-nd/3.0>